Carbon 170 (2020) 270–276

Contents lists available at ScienceDirect

Carbon

journal homepage: www.elsevier.com/locate/carbon

Research Article

Carbon based dots capped tin oxide nanosheets hybridizing with silver nanoparticles for ultra-sensitive surface enhanced raman scattering substrate

Qian Wang [a, b], Mingming Chen [a], Jiaxin Zhang [a], Ting Yu [b, **], FengFu Fu [a, ***], Yongqiang Dong [a, *]

[a] MOE Key Laboratory for Analytical Science of Food Safety and Biology, Fujian Provincial Key Laboratory of Analysis and Detection Technology for Food Safety, College of Chemistry, Fuzhou University, Fuzhou, China
[b] Division of Physics and Applied Physics School of Physical and Mathematical Sciences, Nanyang Technological University, 637371, Singapore

ARTICLE INFO

Article history:
Received 9 June 2020
Received in revised form
27 July 2020
Accepted 30 July 2020
Available online 22 August 2020

Keywords:
Tin oxide
Silver nanoparticles
Carbon based dots
Surface enhanced Raman spectroscopy
Chemical enhancement
Electromagnetic enhancement

ABSTRACT

Carbon based dots capped tin oxide nanosheets (SnO_2/CDs) were synthesized by liquid exfoliation of tin oxide (SnO_2) nanoparticles in the presence of single-layer carbon based (CDs). The obtained SnO_2/CDs have lateral sizes of about 20–50 nm and heights of about 3–4 nm. A thin layer of CDs of about 1–2 nm in thickness are presence on the surface of the SnO_2 nanosheets. The SnO_2/CDs present excellent surface enhanced Raman spectroscopy (SERS) activity due to the chemical enhancement (CM) led by the charge transfer between SnO_2/CDs and the target molecules. The enhancement factor (EF) of the SnO_2/CDs is 1.42×10^5, taking rhodamine 6G as a model target molecule. The SnO_2/CDs are further hybridized with silver nanoparticles (AgNPs) using an in situ synthesis method. The obtained homogeneous nano-hybrids (SnO_2/CDs@AgNPs) have a lot of nanogaps. The nanogaps among the AgNPs/CDs create strong electromagnetic enhancement (EM) due to the "hot spots" effect. The nanogaps among the SnO_2/CDs and AgNPs/CDs allow the target molecules to be embedded, and thus gained both the CM effect of SnO_2/CDs and the EM effect of AgNPs/CDs. As a result, the as-prepared SnO_2/CDs@AgNPs exhibits excellent SERS activities, with an ultrahigh enhancement factor of 3.27×10^{11}.

1. Introduction

As a powerful analytical technique, surface enhanced Raman spectroscopy (SERS) enables single-molecule sensitive detection and provides special chemical fingerprints [1]. It has been extensively applied in many fields such as forensics, homeland security, food safety, and medical diagnostics [2,3]. In SERS, electromagnetic enhancement (EM) and chemical enhancement (CM) are two widely accepted mechanisms [4]. EM refers to the local electromagnetic field effect from the surface plasmon excited by the incident light, while CM originates from the charge transfer (CT) between the target molecule and the substrate [5]. Although the exact mechanism of SERS is still controversial, the SERS signals were absolutely dependent on the substrate. Therefore, great efforts have been made to obtain an ideal SERS substrate during the past decades.

In general, localized EM field is considered to be the dominant contributor to SERS enhancement, which generally has an enhancement factor (EF) of 10^8 or even more [6]. Therefore, various noble metals (e.g. gold, silver, Copper) based nanostructure arrays were designed as SERS substrates [7–11]. However, increasing studies highlight the non-negligible role of CM effect in SERS. Novel SERS substrates with CM effect have been designed, which mainly include graphene based materials and some semiconductor based materials [12–18]. These substrates exhibited EFs higher than 10^5, which is comparable with those of some noble metal based SERS substrates [19]. Recent years, some researchers tried to construct novel SERS substrates integrating both EM and CM effects. Noble metal/semiconductor hybrid nanostructures have attracted board attention acting as SERS-active substrates with higher efficiency by either depositing noble metallic nanostructures on semiconductor

* Corresponding author.
** Corresponding author.
*** Corresponding author.
E-mail addresses: yuting@ntu.edu.sg (T. Yu), fengfu@fzu.edu.cn (F. Fu), dongyq@fzu.edu.cn (Y. Dong).

https://doi.org/10.1016/j.carbon.2020.07.074
0008-6223/

or coating noble metallic nanomaterials with semiconductor [20–26]. However, direct coating noble metallic nanomaterials with a layer of semiconductor would significantly decrease its EM effect due to the increased distance between the probe molecule and the metal surface. Coating the semiconductor with noble metal would inhibit its CM effect since CM effect is usually a "first layer effect" [27]. Consequently, the EF of the reported substrates is usually below 10^9, far below expectation [22–25,28–30]. Therefore, developing a reasonable metal-semiconductor hybrid structure is highly desired for constructing ideal SERS substrates concurrently possessing the EM effect of metal and the CM effect of semiconductor.

In this work, a simple liquid exfoliation method is developed to synthesize carbon based dots capped tin oxide nanosheets (SnO_2/CDs). The obtained SnO_2/CDs show a good SERS activity, with a high EF of 1.42×10^5. Furthermore, the materials can be further hybridized with silver nanoparticles (AgNPs) using a simple and in situ growth method. The obtained nanohybrids (SnO_2/CDs@AgNPs) have a novel sandwich structure. Thus, the target molecules allow to be embedded in the gaps between SnO_2/CDs and AgNPs, and thus gain both the CM effect of SnO_2/CDs and the EM effect of AgNPs. As a result, the as-prepared substrate exhibits an ultrahigh sensitivity of identifying rhodamine 6G (R6G) with concentration as low as 1×10^{-17} M. The EF is as high as 3.27×10^{11}.

2. Experimental section

2.1. Synthesis of CDs

5 g XC-72 carbon black was refluxed with 300 mL concentrated HNO_3 (8.0 M) at 130 °C for 48 h [31]. After the reaction, the suspension was cooled to room temperature then filtered, collecting the filtrate. Finally, about 1.5 g reddish-brown single-layer CDs could be obtained after the filtrate was dried by reduced pressure distillation.

2.2. Synthesis of SnO_2/CDs nano-hybrids

SnO_2/CDs nano-hybrids were prepared by ultrasonic treatment of nano-sized SnO_2 in the presence of CDs. In a typical experiment, 0.6 g SnO_2 powder and 0.6 g single-layer CDs were mixed in 50 mL de-ionized (DI) water, which was ultrasound for 3 h. The as-resulted suspension was centrifuged at 3000 rmp to remove the sediment. Subsequently, the supernatant was further centrifuged at 12,000 rmp to remove the residual CDs, which show good dispersity in the supernatant. Then, the sediment (mainly SnO_2/CDs nano-hybrids) was washed with DI water three times through centrifugation at 12,000 rmp. Finally, the washed SnO_2/CDs nanohybrids were re-dispersed in 10 mL DI water (~5.5 mg/mL) and stored at 4 °C before use.

2.3. Synthesis of SnO_2/CDs@AgNPs nano-hybrids

1.0 mL of SnO_2/CDs solution mentioned above and 300 μL of $AgNO_3$ solution (1.0 M) were added in 50 mL DI water, whose pH value was adjusted to about 8 using $NH_3 \cdot H_2O$ (0.1 M). Then, the suspension was stirred and heated to 80 °C before 5 mL of glucose solution (20 mg/mL) was added. 30 min later, the heating was stopped, allowing the solution cooled naturally to room temperature. Finally, the resulted suspension was centrifuged 12,000 rmp to collect the sediment, which was further washed with DI water twice through centrifugation. The washed SnO_2/CDs@AgNPs nanohybrids were re-dispersed in 10 mL DI water (~1.2 mg/mL) and stored at 4 °C before use.

2.4. Synthesis of AgNPs/CDs

The synthesis of AgNPs/CDs was similar to the experimental procedure of SnO_2/CDs@AgNPs. In brief, 300 μL of $AgNO_3$ (1.0 M) was added to 50 mL CDs solution (0.1 mg/mL), which was subsequently heated to 80 °C. Then 5 mL of glucose solution (20 mg/mL) was added into the solution. The heating was stopped after 30 min, allowing the solution cooled naturally to room temperature under stirring. Finally, the supernatant was collected and washed with DI water through centrifugation at 12,000 rpm. The washed AgNPs/CDs was re-dispersed in DI water and stored at 4 °C.

2.5. SERS detection

SiO_2/Si wafers (0.5×0.5 cm^2) were cleaned by ultrasonic rinsing in acetone, ethanol, and DI water in sequentially. Subsequently, the cleaned SiO_2/Si wafers were immersed in the solution of 98% H_2SO_4/30% H_2O_2 = 4:1 (v/v) for about 4 h, allowing the formation of a hydroxyl surface. Then, hydroxylized SiO_2/Si wafers were further modified with CTAB by being soaked in the solution of 0.05 M CTAB overnight. After that, the SERS substrate materials (20 μL) could be dropped directly on the modified SiO_2/Si wafers, and dried at 60 °C. Finally, the probe molecules (20 μL) were dropped onto the SERS substrates and dried at 60 °C for the SERS measurement.

2.6. Calculation of SERS EFs

The EFs were calculated according to the standard equation:

$$EF = (I_{SERS} / N_{SERS}) / (I_{bulk} / N_{bulk}),$$

where I_{SERS} and I_{bulk} are the SERS intensities of the same vibration mode of the target molecules obtained on the substrates and the normal Raman spectra from solid sample, respectively. N_{SERS} and N_{bulk} represent the numbers of target molecules absorbed on SERS substrates in the focus of the laser beam and the normal Raman sample, respectively. More details about the calculation are shown in the supporting information (see SI).

3. Result and discussion

3.1. Synthesis and characterization of SnO_2/CDs

Nano-sized SnO_2 was ultrasound in the presence of CDs, which were used as the capping agents, to prepare SnO_2/CDs. Transmission electron microscopy (TEM) images indicate that the obtained SnO_2/CDs are nanosheets, whose lateral sizes are distributed in the range of 20–50 nm (Fig. 1A and B). High resolution TEM (HRTEM) image exhibits clear lattice fringes with a spacing of 0.338 nm corresponds to the (110) plane of SnO_2 (Fig. 1C). The lattice structure of SnO_2 nanosheets is further confirmed by the X-ray diffraction (XRD) characterization (Figure S1). However, the edges of the SnO_2 nanosheets (about 1–2 nm in thickness) show nearly no lattice fringe, suggesting the amorphous structure (Fig. 1B and C). High-angle annular dark-field scan TEM (HAADF-STEM) and energy-dispersive X-ray (EDX) results indicate abundant C atoms on the surface of SnO_2 nanosheets (Fig. 1D–F). In other words, the obtained SnO_2 nanosheets are fully covered by CDs to obtain SnO_2 nanosheets core-CDs shell structure. Atomic force microscopy (AFM) images reveal that the height of SnO_2/CDs is in the range of 3–4 nm (Fig. 2). Apparently, the values should contain the thicknesses of the SnO_2 nanosheets and the CDs on them. The thicknesses of the CDs are distributed in the range of 0.3–0.8 nm, with an average of about 0.5 nm (Figure S2). Therefore the thicknesses of the SnO_2 nanosheets should be mainly below 3 nm. Fourier

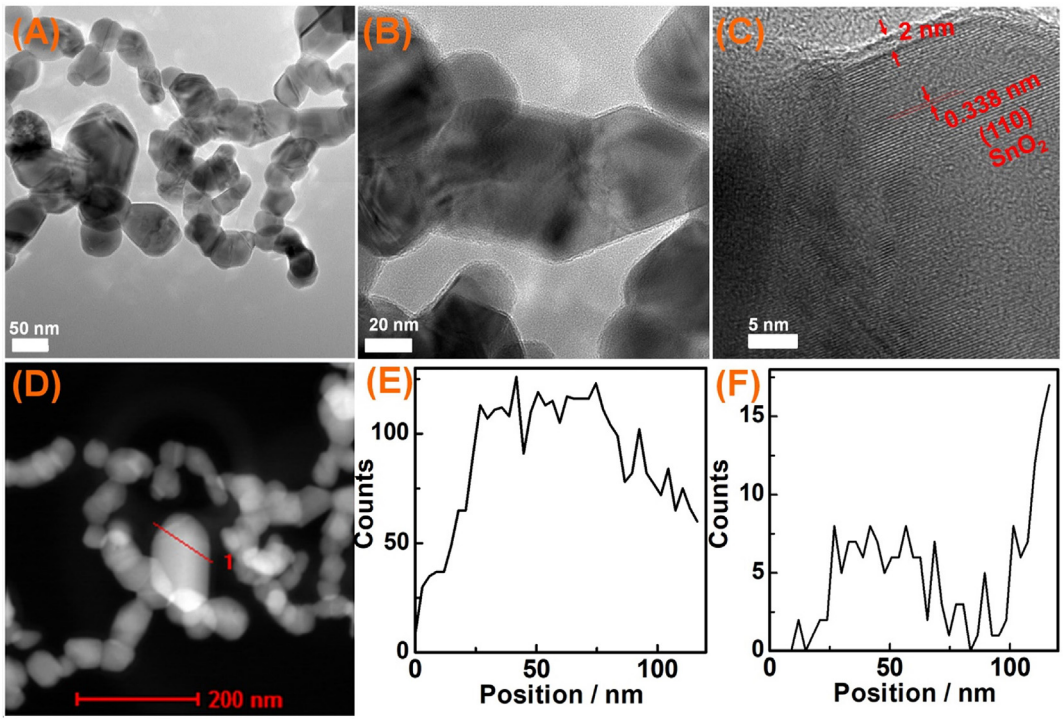

Fig. 1. TEM (A) and HRTEM (B, C) images of SnO_2/CDs, HAADF-STEM image of SnO_2/CDs (D), EDX elemental distribution of C (E) and Sn (F) along the red line in (D). (A colour version of this figure can be viewed online.)

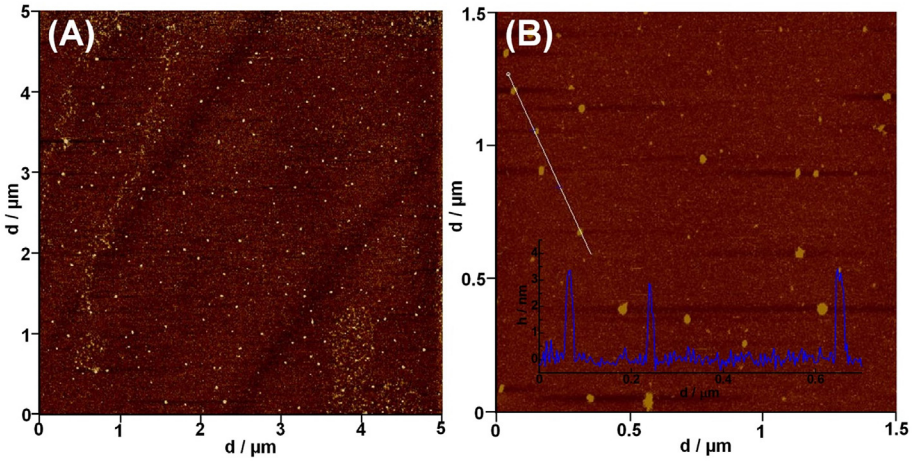

Fig. 2. Atomic force microscopy (AFM) images of SnO_2/CDs with a scale of 5 μm × 5 μm (A) and 1.5 μm × 1.5 μm (B). The inset in (B) is the height profile along the white line in (B). (A colour version of this figure can be viewed online.)

transform infrared (FT-IR) spectra of the obtained SnO_2/CDs exhibit the absorption peaks of C=C, C–OH and O–H bonds from the CDs, and Sn–*O*–Sn bond from the SnO_2 (Figure S3). The results confirm the hybridization of SnO_2 with CDs. It should be mentioned that the relative intensity of the C=O bond of the nanohybrids decrease obviously as compared to that of the pristine CDs. That is because most of the carboxyl groups on CDs are removed after the long-time sonication (It can be further confirmed by the following XPS analysis). However, SnO_2/CDs exhibit excellent and long-term dispersity in water due to the abundant hydroxyl groups and the residual carboxyl groups. In a control experiment, it is found that some SnO_2 nanosheets can also be formed when the nano-sized SnO_2 was ultrasound in the absence of CDs. Furthermore, the morphologies of the obtained SnO_2 nanosheets are quite same with those of SnO_2/CDs (Figure S4), suggesting that the presence of CDs has nearly no effect on the morphologies of SnO_2. However, the SnO_2 nanosheets can't be long-term dispersed in water due to lack of functional groups.

3.2. *SERS activity of SnO_2/CDs*

It was well known, both CDs and many semiconductors could act as SERS substrates due to the CT processes [12,32–34]. Therefore, the obtained SnO_2/CDs may also have a good SERS activity. As shown in Fig. 3, bulk R6G on a SiO_2/Si substrate exhibits very weak Raman signals (curve a), while 1×10^{-5} M R6G on the SnO_2/CDs shows much stronger Raman signal (curve c). Above results confirm the SERS activity of the obtained SnO_2/CDs. The SERS enhancement

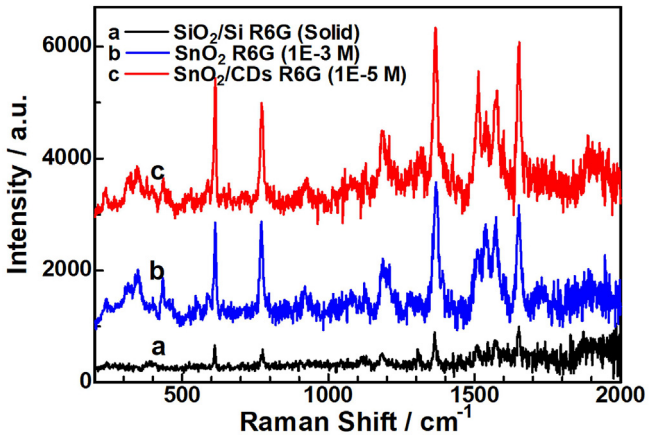

Fig. 3. Raman spectra of R6G on different substrates: bulk R6G on SiO_2/Si (a); 1×10^{-3} M of R6G on SnO_2 (b); and 1×10^{-5} M of R6G on SnO_2/CDs (c). (A colour version of this figure can be viewed online.)

factor (EF) was calculated to be about 1.42×10^5, which is high for a SERS substrate based on the CM effect [12,15,16]. In a control experiment, SnO_2 nanoparticles are also found to be able to work as a SERS substrate with an EF of 1.76×10^3 (curve b), which is much lower than that of SnO_2/CDs. Therefore, the high EF of SnO_2/CDs originates from the synergistic interaction between SnO_2 nanosheets and CDs.

3.3. Synthesis and characterization of SnO_2/CDs@AgNPs

Although the SnO_2/CDs show a good SERS activity, it is still far from an ideal SERS substrate. Therefore, the SnO_2/CDs are further hybridized with AgNPs, which usually exhibit high SERS activities due to the EM properties. In principle, Ag^+ ions are added into the obtained SnO_2/CDs suspension, allowing the Ag^+ absorbed by the oxygen-containing functional groups on the surface of SnO_2/CDs. Then, the absorbed Ag^+ ions are reduced directly by glucose. As a result, SnO_2/CDs@AgNPs nanohybrids are formed. Apparently, the amount of added Ag^+ ions will affect greatly the structure and SERS activity of the obtained materials. Therefore, the amount of Ag^+ is optimized. When the amount of Ag^+ used for the synthesis of SnO_2/CDs@AgNPs substrate is increased from 50 to 300 μL, the surface plasmon resonance (SPR) absorption of AgNPs centered at around 460 nm increases with the increasing amount of Ag^+, without any wavelength-shift (Figure S5). The results indicate that increasing the amount of Ag^+ has nearly no effect on the size of the formed AgNPs, but only increases the amount of the formed AgNPs on the SnO_2/CDs@AgNPs. However, when the amount of Ag^+ is further increased to 400 μL, the SPR absorption of AgNPs and the band-edge absorption of SnO_2 all decrease obviously due to the aggregation of the substrate nanoparticles. Correspondingly, the SnO_2/CDs@AgNPs substrate synthesized at the Ag^+ amount of 300 μL exhibits the strongest SERS signals (Figure S6).

The optimized SnO_2/CDs@AgNPs substrate is characterized in detail. As shown in Fig. 4, the X-ray photoelectron spectroscopy (XPS) analysis exhibits that the obtained SnO_2/CDs@AgNPs nanohybrids are mainly composed of C (43.5 At.%), O (44.6 At.%), Ag (5.3 At.%) and Sn (6.6 At.%). The C_{1s} spectrum reveals the presence of C=C, C–O and C=O bonds. However, the relative intensity of the C=O peak decreases obviously as compared with that of the primary CDs [35]. The results agree well with that from the FTIR spectra. The Sn_{3d} spectrum showed the $Sn_{3d(5/2)}$ and $Sn_{3d(3/2)}$ peaks located at 486.5 and 494.9 eV, ascribing to Sn^{4+} oxidation state [30]. The Ag_{3d} spectrum presents two peaks at 367.6 and 373.6 eV, attributing to $Ag_{3d(5/2)}$ and $Ag_{3(d3/2)}$ of metallic silver, respectively [32]. XRD patterns of the obtained materials exhibit not only the peaks attributed to SnO_2, but also an obvious peak attributed to the (200) crystal facet of Ag at 44.2° (Figure S1). The results indicate that Ag deposited on the surface of SnO_2/CDs nanosheets is in the state of metal Ag (0). TEM images of the resulted materials confirm the formation of a lot of AgNPs with sizes ranging from 30 to 80 nm (Fig. 5A and B). HRTEM images further reveal the crystalline structure of the AgNPs, with a lattice spacing of 0.205 nm corresponding to the (200) plane of Ag (Fig. 5C). Elemental mapping results indicate that the AgNPs are uniformly hybridized with SnO_2/CDs (Fig. 5D–F). Scanning electron microscopy (SEM) images indicate that the morphologies of SnO_2/CDs@AgNPs have no obvious change after being deposited on the CTAB-modified SiO_2/Si wafer (Figure S7).

3.4. SERS performance and mechanism of the as-prepared SnO_2/CDs@AgNPs substrate

The SERS performance of the obtained SnO_2/CDs@AgNPs substrate is evaluated by using R6G as the probe molecule. Fig. 6A shows the SERS spectra of R6G with various concentrations from 1.0×10^{-17} to 1.0×10^{-12} M. The Raman peaks of R6G can be clearly observed even at a concentration of 1×10^{-17} M. There is a good semi-logarithmic correlation between the Raman intensity at 1655 cm^{-1} and the concentration of R6G (Fig. 6B). The EF is calculated to be 3.27×10^{11}. In addition, the obtained SERS substrate exhibits good spectral uniformity and repeatability (Figure S8). Apparently, the synthesized SnO_2/CDs@AgNPs is an excellent SERS substrate.

The possible enhancement mechanism of the SnO_2/CDs@AgNPs SERS substrate is clarified. As well known that the gapped AgNPs would create electromagnetic “hot-spots” to generate strong local electromagnetic field and thus significantly enhance the SERS effects. The HRTEM images of the substrate mentioned above indicate that the formed AgNPs are gapped from each other with a thin layer of CDs, whose thickness is only about 1 nm. Apparently, the substrate exhibited outstanding SERS effects due to the strong EM from the gapped AgNPs. In a control experiment, AgNPs/CDs were synthesized for SERS investigation (Figure S9). Strong SERS signal of R6G could be detected even at concentration lower than 1×10^{-9} M (Figure S10), the result is comparable with those of other metallic nanostructures [8,10,11,36]. On one hand, the results confirmed the SERS activity of AgNPs/CDs. On the other hand, the fact that the SERS activity of AgNPs/CDs is much lower than that of SnO_2/CDs@AgNPs implied that the CM effect of SnO_2/CDs is quite important for the SnO_2/CDs@AgNPs substrate, and should be further discussed.

It is found that the SERS performance of the obtained SnO_2/CDs@AgNPs is greatly dependent on the excitation wavelength. The SERS signals excited at 532 nm are much stronger than those excited at 633 and 785 nm (Figure S11). The result might be related to the relative strong SPR absorption of AgNPs at 532 nm (Figure S5). However, the CT between R6G and SnO_2 could also be the key factor for the effect of excitation wavelength (Fig. 7A). The conduction band (CB) of SnO_2/CDs is measured to be ~ -4.50 eV (Figure S12), and the band gap to be ~3.50 eV (Figure S13). Then the valence band (VB) would be −8.00 eV. The results fit well with those of SnO_2 [37], indicating that the coating of CDs has no obvious effect on the CB and VB of SnO_2. For R6G molecule, the highest occupied molecule orbital (HOMO) and the lowest unoccupied molecule orbital (LUMO) are −5.70 and −3.40 eV, respectively [14]. When the excitation wavelength is 532 nm (~2.33 eV), electron transition from HOMO to LUMO of the R6G molecule happens, then CT process from LUMO of the R6G molecule to CB of SnO_2/CDs (CT1)

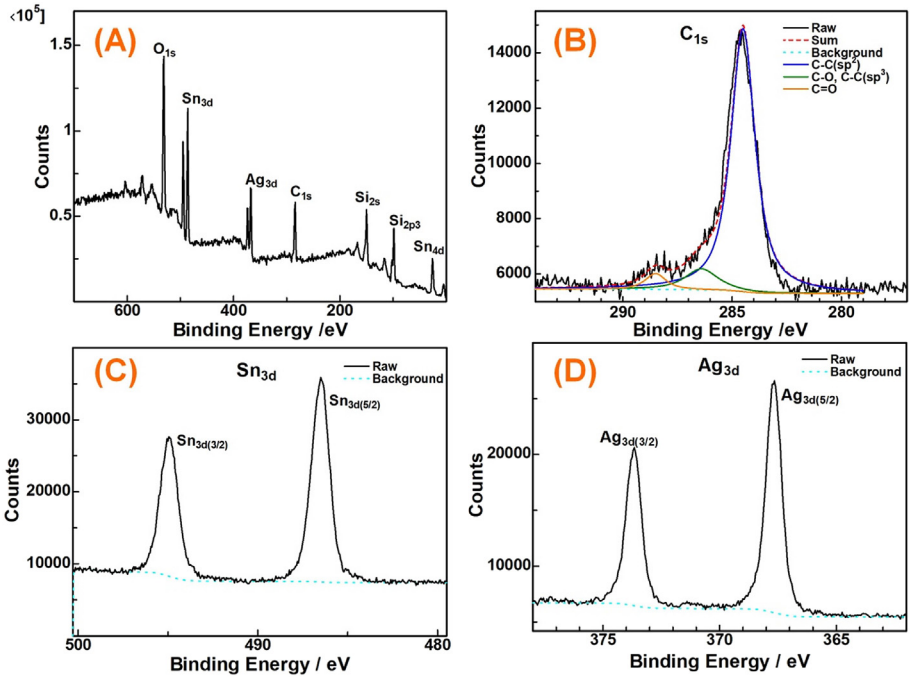

Fig. 4. XPS spectrum of SnO_2/CDs@AgNPs (a), high resolution XPS spectra of C_{1s} (b), Sn_{3d} (c), and Ag_{3d} (d). (A colour version of this figure can be viewed online.)

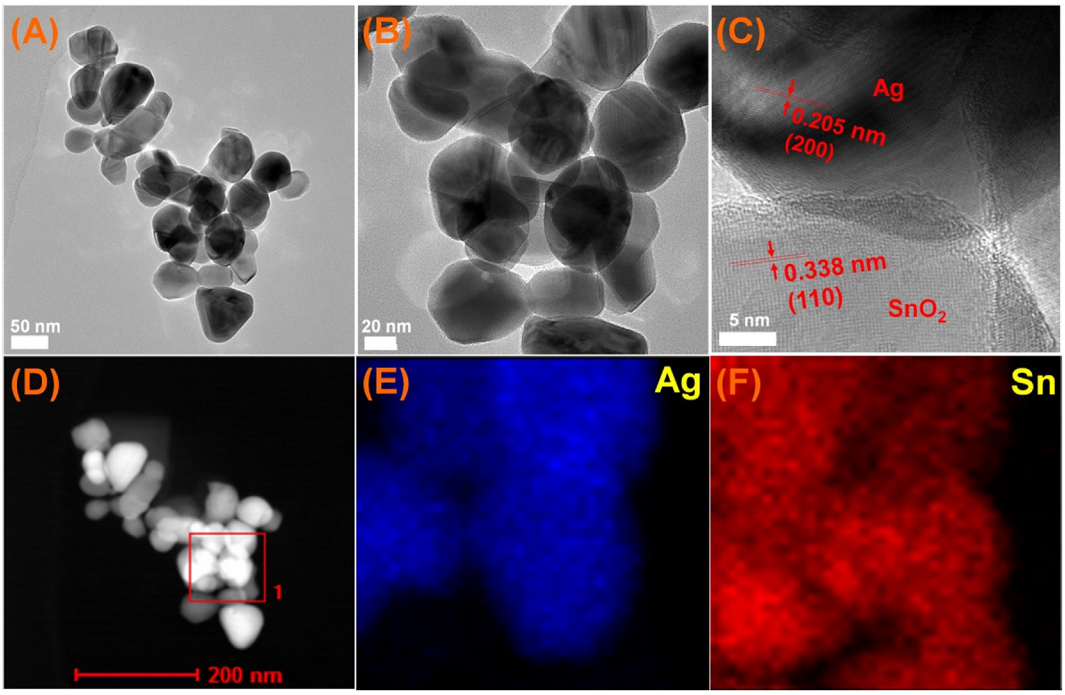

Fig. 5. TEM (A, B), HRTEM (C), and HAADF-STEM (D) images of SnO_2/CDs@AgNPs, and the corresponding (the area framed in D) EDX elemental maps of C (E) and Sn (F). (A colour version of this figure can be viewed online.)

occurs. Meanwhile, CT process from the HOMO of R6G molecule to the CB of SnO_2/CDs (CT2) is also thermodynamically feasible. As a result, the polarizability tensor of R6G can be strongly magnified, bringing out an evident Raman enhancement. When increasing the excitation wavelength to 633 nm (~1.96 eV), CT1 is inhibited while CT2 is still thermodynamically allowed. However, CT2 is usually difficult on the SERS substrate because of no molecular orbital coupling of R6G with SnO_2. Therefore, the SERS intensity is decreased obviously when compared with that excited at 532 nm. Finally, when further increasing the excitation wavelength to 785 nm (1.58 eV), both CT1 and CT2 are thermodynamically inhibited. Accordingly, the SERS intensity is further decreased. The results indicate that the CM effect from SnO_2/CDs is important for the SERS substrate.

To further confirm the role of CM effect from SnO_2/CDs, crystal violet (CV) and 4-aminothiophenol (4-ATP) are used as the probe

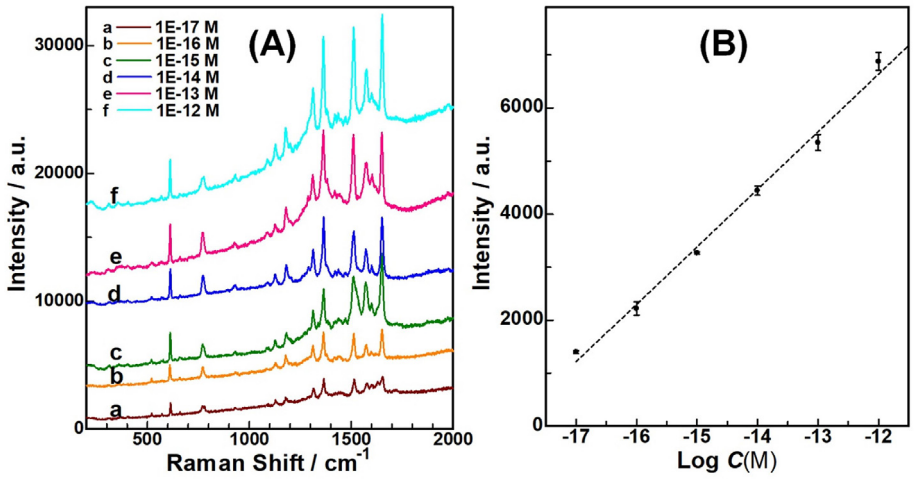

Fig. 6. Raman spectra of various concentrations of R6G on SnO_2/CDs@AgNPs substrate. All the Raman spectra were obtained under excitation of 532 nm (A). The linear relationship between the logarithmic intensities (1655 cm^{-1}) and the R6G concentrations (B). (A colour version of this figure can be viewed online.)

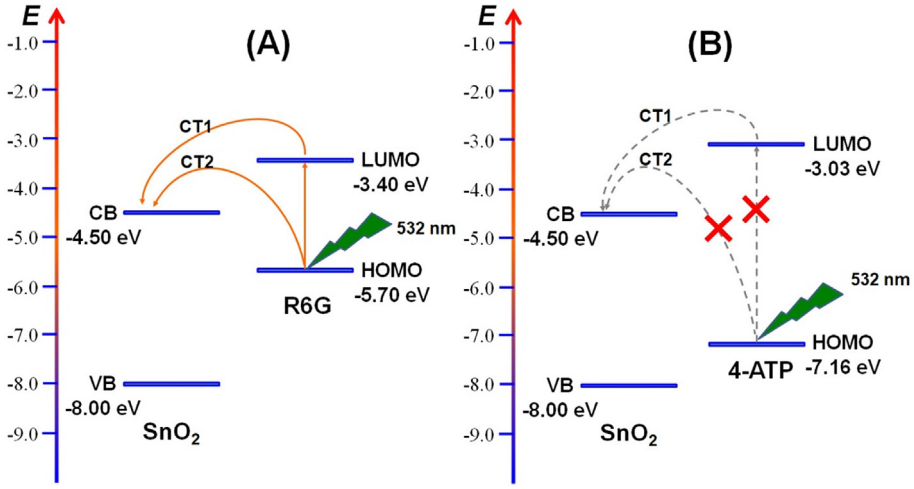

Fig. 7. Schematic diagram illustrating the thermodynamically allowed CT process between the R6G molecule and SnO_2/CDs (A). Schematic illustration of the thermodynamically forbidden CT process between the 4-ATP molecule and SnO_2/CDs (B). (A colour version of this figure can be viewed online.)

molecules to decorate the obtained SERS substrate. The LUMO and HOMO of CV are −4.10 eV and −6.00 eV, respectively [39]. Apparently, the energy levels of CV are similar with those of R6G. As expected, the SERS signals of CV can still be clearly detected even at an ultralow concentration of 1×10^{-16} M (Figure S14). There is a linear relationship between the logarithmic Raman peak intensity of 1621 cm^{-1} and the concentration of CV. Different from R6G and CV, the LUMO and HOMO of 4-ATP are −3.03 and −7.16 eV, respectively [38]. Both the two CT processes are thermodynamically inhibited under the excitation of the three wavelengths (Fig. 7B). In other words, the CM effect from SnO_2/CDs does not work for 4-ATP. As a result, the SERS intensities of 4-ATP on SnO_2/CDs@AgNPs are much weaker (Figure S15). The results mentioned above indicate that the CM effect from SnO_2/CDs is important for an excellent SERS substrate. Furthermore, matching the HOMO and LUMO of the attached molecules to the CB and VB of the semiconductor is the key factor to gain the CM effect, and received high SERS signals. The results indicate that the obtained SnO_2/CDs@AgNPs integrate the CM effect of SnO_2/CDs and the EM effect AgNPs/CDs, and thus exhibit excellent SERS activities. The combination of EM and CM effects may be related to the special structure of the materials. It can be clearly seen from the HRTEM image of the materials that a lot of gaps are presented between AgNPs/CDs and SnO_2/CDs, allowing the target molecules adsorbed. Then, the adsorbed molecules can gain both the CM effect of SnO_2/CDs and the EM effect of AgNPs/CDs.

4. Summary

In conclusion, we herein design and fabricate a novel substrate by integrating SnO_2 nanosheets, single-layer CDs and AgNPs for ultrasensitive SERS analysis. The prepared SnO_2/CDs@AgNPs combine the CM effect of SnO_2/CDs and EM effect of AgNPs/CDs, and thus exhibit outstanding SERS activity and repeatability. By using SnO_2/CDs@AgNPs as SERS substrate, a concentration as low as 1.0×10^{-17} M of R6G of can still be clearly identified by SERS. The SERS EF of the proposed substrate is calculated to be 3.27×10^{11}. The outstanding SERS activity and repeatability of the proposed substrate show promising applications in on-site sensing or rapid detection of ultralow-concentration of organic pollutant. More importantly, the present work guides future development in structure design and fabrication of high-performance SERS substrate.

CRediT authorship contribution statement

Qian Wang: Formal analysis, Writing - original draft. **Mingming Chen:** Formal analysis, Writing - original draft. **Jiaxin Zhang:** Formal analysis, Writing - original draft. **Ting Yu:** Supervision. **FengFu Fu:** Supervision. **Yongqiang Dong:** Supervision.

Declaration of competing interest

The authors declare that they have no known competing financial interests or personal relationships that could have appeared to influence the work reported in this paper.

Acknowledgment

This study was financially supported by National Key Research and Development Program of China (2017YFC1600500), National Natural Science Foundation of China (21675026, 21976029), Singapore Ministry of Education (MOE Tier 2 MOE2018-T2-2-072), and the Program for Changjiang Scholars and Innovative Research Team in University (No. IRT1116).

Appendix A. Supplementary data

Supplementary data to this article can be found online at https://doi.org/10.1016/j.carbon.2020.07.074.

References

[1] S. Nie, S.R. Emory, Probing single molecules and single nanoparticles by surface-enhanced Raman scattering, Science 275 (5303) (1997) 1102–1106.
[2] J.F. Li, Y.F. Huang, Y. Ding, Z.L. Yang, S.B. Li, X.S. Zhou, et al., Shell-isolated nanoparticle-enhanced Raman spectroscopy, Nature 464 (2010) 392–395.
[3] I. Alessandri, J.R. Lombardi, Enhanced Raman scattering with dielectrics, Chem. Rev. 116 (24) (2016) 14921–14981.
[4] A. Campion, P. Kambhampati, Surface-enhanced Raman scattering, Chem. Soc. Rev. 27 (4) (1998) 293–312.
[5] A. Otto, The 'chemical' [electronic] contribution to surface-enhanced Raman scattering, J. Raman Spectrosc. 36 (2005) 497–509.
[6] G.C. Schatz, M.A. Young, R.P.V. Duyne, Electromagnetic mechanism of SERS, Top. Appl. Phys. 103 (2006) 19–46.
[7] X. Li, J. Li, X. Zhou, Y. Ma, Z. Zheng, X. Duan, et al., Silver nanoparticles protected by monolayer graphene as a stabilized substrate for surface enhanced Raman spectroscopy, Carbon 66 (2014) 713–719.
[8] Y. Dong, Q. Wang, L. Wan, X. You, Y. Chi, Carbon based quantum dots capped silver nanoparticles for efficient surface-enhanced Raman scattering sensing, J. Mater. Chem. C 4 (31) (2016) 7472–7477.
[9] A. Liu, T. Xu, J. Tang, H. Wu, T. Zhao, W. Tang, Sandwich-structured Ag/graphene/Au hybrid for surface-enhanced Raman scattering, Electrochim. Acta 119 (2014) 43–48.
[10] W. Fan, Y.H. Lee, S. Pedireddy, Q. Zhang, T. Liu, X.Y. Ling, Graphene oxide and shape-controlled silver nanoparticle hybrids for ultrasensitive single-particle surface-enhanced Raman scattering [SERS] sensing, Nanoscale 6 (9) (2014) 4843–4851.
[11] P. Luo, C. Li, G. Shi, Synthesis of gold@carbon dots composite nanoparticles for surface enhanced Raman scattering, Phys. Chem. Chem. Phys. 14 (20) (2012) 7360–7366.
[12] Z. Zheng, S. Cong, W. Gong, J. Xuan, G. Li, W. Lu, et al., Semiconductor SERS enhancement enabled by oxygen incorporation, Nat. Commun. 8 (1) (2017) 1993.
[13] W. Xu, X. Li, J. Xiao, M.S. Dresselhaus, J. Kong, H. Xu, et al., Surface enhanced Raman spectroscopy on a flat graphene surface, P. Natl. Acad. Sci. USA 109 (24) (2012) 9281–9286.
[14] X. Ling, L. Xie, Y. Fang, H. Xu, H. Zhang, J. Kong, et al., Can graphene be used as a substrate for Raman enhancement? Nano Lett. 10 (2) (2010) 553–561.
[15] X. Wang, W. Shi, Z. Jin, W. Huang, J. Lin, G. Ma, et al., Remarkable SERS activity observed from amorphous ZnO nanocages, Angew. Chem. Int. Ed. 56 (33) (2017) 9851–9855.
[16] J. Lin, Y. Shang, X. Li, J. Yu, X. Wang, L. Guo, Ultrasensitive SERS detection by defect engineering on single Cu_2O superstructure particle, Adv. Mater. 29 (5) (2017) 1604797.
[17] H. Wu, H. Wang, G. Li, Metal oxide semiconductor SERS-active substrates by defect engineering, Analyst 142 (2) (2017) 326–335.
[18] S. Huh, J. Park, Y.S. Kim, K.S. Kim, B.H. Hong, et al., UV/ozone-oxidized large-scale graphene platform with large chemical enhancement in surface-enhanced Raman scattering, ACS Nano 5 (12) (2011) 9799–9806.
[19] S. Cong, Y. Yuan, Z. Chen, J. Hou, M. Yang, Y. Su, et al., Noble metal-comparable SERS enhancement from semiconducting metal oxides by making oxygen vacancies, Nat. Commun. 6 (2015) 7800.
[20] C. Tan, Z. Zhang, Y. Qu, L. He, Ag_2O/TiO_2 nanocomposite heterostructure as a dual functional semiconducting substrate for SERS/SEIRAS application, Langmuir 33 (22) (2017) 5345–5352.
[21] L. Liu, H. Yang, X. Ren, J. Tang, Y. Li, X. Zhang, et al., Au-ZnO hybrid nanoparticles exhibiting strong charge-transfer-induced SERS for recyclable SERS-active substrates, Nanoscale 7 (12) (2015) 5147–5151.
[22] J. Huang, D. Ma, F. Chen, D. Chen, M. Bai, K. Xu, Green in situ synthesis of clean 3D chestnutlike Ag/WO_{3-x} nanostructures for highly efficient, recyclable and sensitive SERS sensing, ACS Appl. Mater. Inter. 9 (8) (2017) 7436–7446.
[23] W. Song, X. Han, L. Chen, Y. Yang, B. Tang, W. Ji, et al., Site-specific deposition of Ag nanoparticles on ZnO nanorod arrays via galvanic reduction and their SERS applications, J. Raman Spectrosc. 41 (9) (2010) 907–913.
[24] X. He, C. Yue, Y. Zang, J. Yin, S. Sun, J. Li, et al., Multi-hot spot configuration on urchin-like Ag nanoparticle/ZnO hollow nanosphere arrays for highly sensitive SERS, J. Mater. Chem. 1 (47) (2013) 15010–15015.
[25] X. Liang, Y. Wang, T. You, X. Zhang, N. Yang, G. Wang, et al., Interfacial synthesis of a three-dimensional hierarchical MoS_2-NS@Ag-NP nanocomposite as a SERS nanosensor for ultrasensitive thiram detection, Nanoscale 9 (25) (2017) 8879–8888.
[26] G. Oldfield, T. Ung, P. Mulvaney, $Au@SnO_2$ core-shell nanocapacitors, Adv. Mater. 12 (20) (2000) 1519–1522.
[27] A. Otto, I. Mrozek, H. Grabhorn, W. Akemann, Surface-enhanced Raman scattering, J. Phys. Condens. Matter 4 (5) (1992) 1143–1212.
[28] H. Tang, G. Meng, Q. Huang, Z. Zhang, Z. Huang, C. Zhu, Arrays of cone-shaped ZnO nanorods decorated with Ag nanoparticles as 3D surface-enhanced Raman scattering substrates for rapid detection of trace polychlorinated biphenyls, Adv. Funct. Mater. 22 (1) (2012) 218–224.
[29] H. Fu, X. Lang, C. Hou, Z. Wen, Y. Zhu, M. Zhao, et al., Nanoporous Au/SnO/Ag heterogeneous films for ultrahigh and uniform surface-enhanced Raman scattering, J. Mater. Chem. C 2 (35) (2014) 7216–7222.
[30] B. Liu, W. Zhang, H. Lv, D. Zhang, X. Gong, Novel Ag decorated biomorphic SnO_2 inspired by natural 3D nanostructures as SERS substrates, Mater. Lett. 74 (2012) 43–45.
[31] Y. Dong, C. Chen, X. Zheng, L. Gao, Z. Cui, H. Yang, et al., One-step and high yield simultaneous preparation of single- and multi-layer graphene quantum dots from CX-72 carbon black, J. Mater. Chem. 22 (40) (2012) 8764–8766.
[32] L. Yang, X. Jiang, W. Ruan, J. Yang, B. Zhao, W. Xu, Charge-transfer-induced surface-enhanced Raman scattering on $Ag\text{-}TiO_2$ nanocomposites, J. Phys. Chem. C 113 (36) (2009) 16226–16231.
[33] E. Fazio, F. Neri, S. Savasta, S. Spadaro, S. Trusso, Surface-enhanced Raman scattering of SnO_2 bulk material and colloidal solutions, Phys. Rev. B 85 (19) (2012) 195423.
[34] H. Cheng, Y. Zhao, Y. Fan, X. Xie, L. Qu, G. Shi, Graphene-quantum-dot assembled nanotubes: a new platform for efficient Raman enhancement, ACS Nano 6 (3) (2012) 2237–2244.
[35] M. Wang, R. Sun, Q. Wang, L. Chen, L. Hou, Y. Chi, Effects of C-related dangling bonds and functional groups on the fluorescent and electrochemiluminescent properties of carbon-based dots, Chem. Eur J. 24 (17) (2018) 4250–4254.
[36] Y. Fan, H. Cheng, C. Zhou, X. Xie, Y. Liu, L. Dai, Honeycomb architecture of carbon quantum dots: a new efficient substrate to support gold for stronger SERS, Nanoscale 4 (5) (2012) 1776–1781.
[37] W.W. Wang, Y.J. Zhu, L.X. Yang, $ZnO–SnO_2$ hollow spheres and hierarchical nanosheets: hydrothermal preparation, formation mechanism, and photocatalytic properties, Adv. Funct. Mater. 17 (1) (2007) 59–64.
[38] M.V. Cañamares, C. Chenal, R.L. Birke, J.R. Lombardi, DFT, SERS, and single-molecule SERS of crystal violet, J. Phys. Chem. C 112 (51) (2008) 20295–20300.
[39] Z. Sun, C. Wang, J. Yang, B. Zhao, J.R. Lombardi, Nanoparticle metal-semiconductor charge transfer in ZnO/PATP/Ag assemblies by surface-enhanced Raman spectroscopy, J. Phys. Chem. C 112 (15) (2008) 6093–6098.